Applied Radiation and Isotopes 206 (2024) 111227

Contents lists available at ScienceDirect

Applied Radiation and Isotopes

journal homepage: www.elsevier.com/locate/apradiso

Designing lightweight neutron absorbing composites using a comprehensive absorber areal density metric

Andrew O'Connor [a], Cheol Park [b], Wesley E. Bolch [a], Andreas Enqvist [a], Michele V. Manuel [a,*]

[a] University of Florida, Gainesville, FL, USA
[b] NASA Langley Research Center, Hampton, VA, USA

ARTICLE INFO

Keywords:
Metal matrix composite
Neutron channeling
Monte Carlo radiation transport
Neutron absorption testing
boron-10 equivalent areal density
Lightweight magnesium alloys

ABSTRACT

Efforts to lightweight neutron absorbing composites are limited by incomplete understandings of the interaction between absorbing particles and their matrices. In this study, analytical models and a more physically representative simulation evaluated the penalty to neutron absorbing performance due to neutron channeling between large absorbing particles. Models and simulation agreed that B_4C particles smaller than 100μm and especially those smaller than 10μm did not cause excessive neutron channeling. A more comprehensive neutron absorbing composite design metric – boron-10 equivalent areal density, which considers the particle size penalty and the matrix contribution to absorptivity – was introduced and used to estimate lightweighting via matrix substitution. Calculations using this new metric showed that a non-absorbing Mg matrix reduced mass by up to 35% over Al, constrained by the difference in mass density, while an absorbing Mg–Li matrix reduced mass by up to 60%, exceeding the difference in mass densities alone. Measurement of apparent absorber areal density through two experimental techniques – foil activation and direct counting – validated estimated absorber areal density as a neutron absorbing composite design metric. This updated understanding of the particle size penalty, newly introduced design metric, and experimental validation demonstrate a path to lightweight neutron absorbing composites.

1. Introduction

Neutron absorbing composites (NACs) are useful in a variety of terrestrial and aerospace applications where neutron radiation is a concern: as criticality control for used nuclear fuel casks (Machiels and Lambert, 2009) and as shielding for a variety of use cases which include particle accelerators (Cecchetto et al., 2020), nuclear medicine procedures (Afkham et al., 2020), nuclear power sources (Athanasakis et al., 2020), space nuclear propulsion (Caffrey et al., 2015), high-altitude aviation (ICRP, 2016; Singleterry and Thibeault, 2000), and space exploration missions (ICRP, 2013; Thibeault et al., 2015; Naito et al., 2021). NACs are typically metal or polymeric matrices reinforced with neutron absorbing materials, often as discontinuous particles (Fu et al., 2021; Tamayo et al., 2020). As most neutron absorbing nuclides have poor mechanical properties, the matrix provides structural framework for absorbing reinforcements. The absorbing reinforcements are commonly boron-containing, most often boron carbide (B_4C) due to its combination of good strengthening, high thermal stability, and excellent low-energy (thermal) neutron absorptivity (Park et al., 2015; Chen et al., 2015; Li et al., 2017).

While existing NACs often are composed of aluminum (Al) matrices (Chen et al., 2015; Park et al., 2015; Li et al., 2017; Zhang et al., 2013; Lee et al., 2021; Zhang et al., 2019), lightweight matrices like magnesium (Mg) or magnesium-lithium (Mg–Li) alloys could reduce their mass while maintaining structural utility and mitigating space radiation (O'Connor et al., 2024), thus improving their suitability for mass-constrained applications such as aerospace (Belvin et al., 2006). Designing and evaluating lightweight, structural NACs is thus of interest for shielding neutron-rich environments, especially in aerospace applications.

Before fabricating NACs, the reinforcement material and morphology – especially its particle size – must be chosen. Large particles tend to allow neutrons, especially thermal ones, to stream between the large spaces between them without being absorbed: the neutron channeling effect (Burrus, 1958; Smith, 1948; Wells et al., 1987). Thus, actual NAC performance will be lower than expected based on composition alone. Using smaller particles ameliorates this effect (Smith, 1948; Burrus, 1958; Schrempp-Koops, 2013), but decreasing particle size makes fabrication more difficult, primarily due to particle agglomeration and

* Corresponding author.
E-mail addresses: a.oconnor@ufl.edu (A. O'Connor), cheol.park-1@nasa.gov (C. Park), wbolch@ufl.edu (W.E. Bolch), enqvist@ufl.edu (A. Enqvist), mmanuel@ufl.edu (M.V. Manuel).

https://doi.org/10.1016/j.apradiso.2024.111227
Received 23 July 2023; Received in revised form 28 January 2024; Accepted 4 February 2024
Available online 5 February 2024

clustering (Malaki et al., 2019). As such, the chosen particle size must balance the loss of shielding efficiency due to neutron channeling with any increased difficulty of fabrication.

Several analytical and computational models can be used to investigate the particle size effect on neutron absorptivity from neutron channeling. Early analytical modes employed Coveyou's conception of neutrons streaming between absorbing chunks subdivided into layers approximating the particle size in NACs (Smith, 1948; Burrus, 1958, 1960; Åkerhielm, 1960). Later analytical models employed nuclear fuel homogenization methods (Shmakov et al., 2000; Yamamoto, 2006; Yamamoto et al., 2006; Yamamoto, 2010) or semi-classical approximations (Schrempp-Koops, 2013) to determine the particle size effect. These models typically indicated that B_4C particles less than hundreds of microns were acceptable in NACs. These analytical models are useful for larger, micron-sized particles but sometimes yield inconsistent results in the nanometer range.[1] This may be due to any number of assumptions and simplifications inherent to these models. Most notably, scattering and absorption in the matrix is neglected. As such, Monte Carlo radiation transport simulations – that account for a variety of physical phenomena – were conducted to validate the trend in decreasing neutron absorptivity with increasing particle size. Past simulations of NACs were not physically realistic: they employed periodic arrangements of absorbing particles (Basturk et al., 2005; Dyrnjaja and Zawisky, 2015; Turner, 2005; Soltani et al., 2016; Kim et al., 2014) whereas real NACs ideally have random spacing between particles. Thus, these models tended to suggest that nano-sized B_4C particles were needed to avoid significant neutron channeling. As such, the present study used a more physically representative microstructure in simulating NACs. By validating the particle size effect, it can be accounted for during NAC design.

A NAC must be designed to a particular neutron absorbing performance to match its intended application. Absorber areal density is one such metric used to predict neutron absorbing performance (Li et al., 2017; Jiang et al., 2019; O'Connor et al., 2020). Especially when considering lightweight NACs with neutron absorbing matrices, more comprehensive design metrics are needed to predict the expected mass reductions. This study introduces a NAC design metric using areal density that accounts for the contributions of discontinuous absorbers (particles) subject to size penalties from neutron channeling and those of continuous absorbers not subject to them. This metric was then used to evaluate the potential lightweighting of NACs by matrix substitution with less mass dense metals such as Mg and Mg–Li.

Previous introductions of absorber areal densities as NAC design metrics did not provide experimental validation (Li et al., 2017; Jiang et al., 2019). And when the neutron performance of NACs is measured, it is often reported as macroscopic cross-sections or neutron transmission ratios (Park et al., 2015; Chen et al., 2016) instead of areal density, confounding efforts to compare differing NACs. This study compares theoretical absorber areal density (boron-10 equivalent areal density (^{10}BEAD)) to that measured by two separate neutron absorption testing setups. These were an In foil activation method modified to correct for changes in incident neutron fluence, background radiation, and non-thermal neutrons as recommended by the relevant ASTM standard (E07 Committee, 2020) and a confirmatory direct counting method more similar to the ASTM standard. The results from these setups indicate the validity of the techniques and the use of absorber areal density as a NAC metric.

This present study computationally predicts the particle size penalty for B_4C with comparison to analytical models, introduces a more comprehensive absorber areal density calculation, illustrates lightweighting via matrix substitution as computed by this updated design metric, and finally experimentally validates absorber areal density as a NAC design metric.

[1] With the notable exception of Schrempp-Koops (2013).

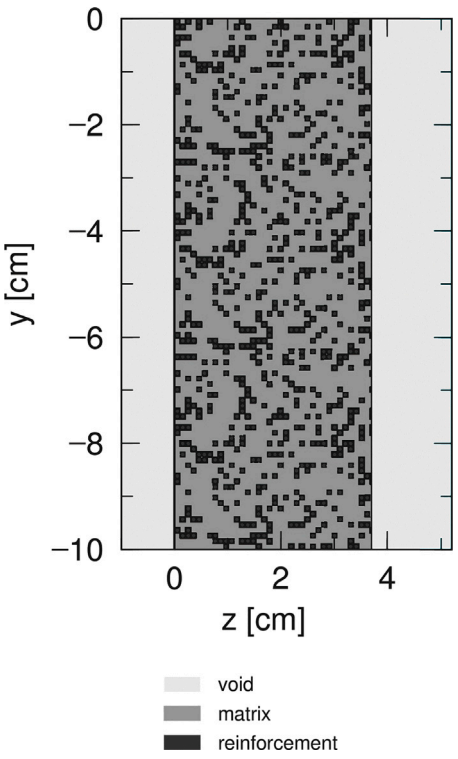

Fig. 1. Illustrative cross-section of a pseudo-random particle distribution in PHITS.

2. Materials and methods

Analytical models based on differing methodology (Smith, 1948; Shmakov et al., 2000) were chosen to compute neutron shielding efficiency by particle size. The PHITS (Sato et al., 2018) version 3.26 – a Monte Carlo radiation transport code – was chosen for its flexibility, ability to use advanced geometries such as nested universes and repeating lattices, ease of ingesting external data, and inclusion of neutron interactions such as scattering. A 5 cm radius right cylinder with a radial periodic boundary condition and a thickness set to an areal density of 10 g cm^{-2} represented a prototypical NAC. The neutron source was a 5 cm disc coaxial with the prototypical NAC set to emit monoenergetic 25 meV neutrons isotropically. Unless otherwise specified, all simulations used an Al matrix reinforced with monodisperse 10 μm diameter B_4C spheres at 10% by volume. Reinforcements were modeled as spherical particles at the center of a box with the same dimensions as their diameter. An in-house Python script generated pseudo-random distributions of cells containing either matrix alone or matrix and particle, populated according to the reinforcement volume fraction. With especially small reinforcements, PHITS required excessive computer memory. As such, a technique using nested universes and lattices reduced the computational burden while retaining accuracy. The same Python script generated 100 by 100 by 100 lattices to provide appropriate randomness. These "sublattices" were then nested into a larger, repeating lattice comprising the entire simulated NAC volume. Fig. 1 depicts an example cross-section of this geometry.

2.1. Experimental

Experimental measurements of neutron absorption, giving a measured boron-10 areal density (^{10}BAD), were conducted in a manner inspired by the ASTM E2971-16 standard (E07 Committee, 2020). Previously fabricated Mg and Mg–Li matrix, B_4C-reinforced NAC specimens with 2 cm by 2 cm cross-sectional area were machined to a constant thickness of 2.5 mm. Calibration standards were Mg–Li alloys

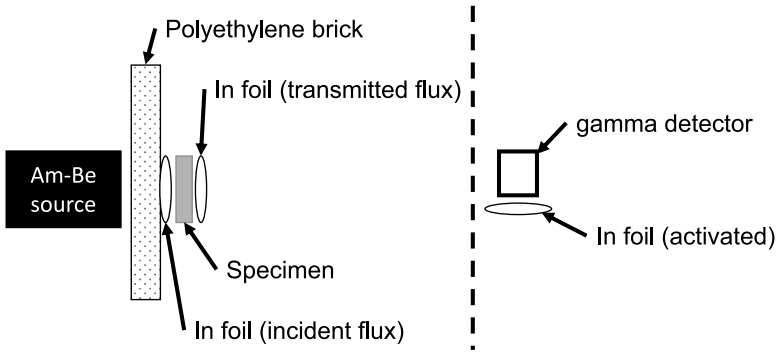

Fig. 2. Diagram of foil activating and counting setup.

with a known isotopic ratio (95.4%) of the absorbing ^{6}Li isotope.[2] The low and high areal density specimens had their compositions verified by inductively coupled plasma - optical emission spectroscopy (ICP-OES) as Mg-2.0wt%Li and Mg-7.96wt%Li, respectively.

2.1.1. Foil activation setup

For the foil activation setup shown in Fig. 2, a 3.564×10^{10} Bq americium-beryllium (Am–Be) fast neutron source was fixed into an assembly of lead bricks for shielding. Separately, a specimen holder consisting of a 25 mm-thick block of polyethylene and retaining clips was prepared. A 1 in-diameter indium (In) foil was placed immediately after the polyethylene to measure the incident neutron beam power.[3] This was followed by the ostensibly absorbing specimen. This setup was used in previous literature reports (Kang et al., 2015; Bacca et al., 2022). Unique to this study, another In foil was placed after the specimen to measure the transmitted neutrons. The assembled specimen holder was placed immediately adjacent to the neutron source with the polyethylene moderator between the source and specimen to produce sufficient thermalized neutrons. An irradiation time of 6 h activated the In foils to 99% saturation.

After irradiation, the specimen holders were removed from the leaded assembly and moved to a separate room for counting. To measure their activity and thus neutron counts, the In foils were removed from the specimen holder and each counted by separate Geiger-Müeller (G-M) tubes (Spectrum Techniques GM35). The G-M tubes were independently powered and monitored by separate counters (Spectrum Techniques ST360) connected to independent computers recording the accumulated counts in the STX software (Spectrum Technologies). The foils were counted in periods of 100 s counting and 20 s resting for a total of 2 h, after which the foils had decayed to such a level that had excessive uncertainty in the counts. Background counts were taken for 2 h after each specimen finished counting.

2.1.2. Direct counting setup

For the direct counting setup shown in Fig. 3, a 9.1×10^{5} Bq californium-252 (^{252}Cf) fast neutron source was placed in a polyethylene barrel to thermalize emitted neutrons. The test specimens were placed immediately adjacent to the barrel and within a 4 cm^2 shroud of cadmium (Cd) foil (1 mm thick; 99.99% pure, assumed natural isotopic abundance; Goodfellow Corporation) to reduce scattering into the detector. The helium-3 (^{3}He) neutron detector (Saint-Gobain tube with associated Precision Data Technologies PDT20A-HN-5V electronics) was placed after the test specimen and powered (HP E3610A) with its output directed to a counter/timer (ORTEC 974 Quad). The detector tube itself was wrapped with the same Cd foil as the shroud to reduce background and scattered neutron counts, except for a 4 cm^2 opening

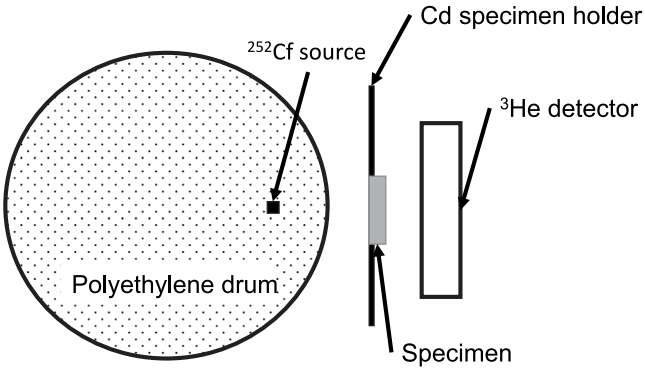

Fig. 3. Direct counting setup diagram.

coaxial with the test specimen. Due to the relatively short half-life of ^{252}Cf (2.645 a), the source's activity decayed noticeably to 8.0×10^{5} Bq, approximately 88% of the initial activity, by the end of the period. This constantly decreasing activity and thus incident beam power were accounted for by measuring the specimen-incident neutron flux without a specimen present for 1 h prior to each specimen irradiation.

3. Theory

3.1. Areal density

Areal density including boron-10 alone. Li et al. (2017) introduced boron-10 areal density (^{10}BAD) as a geometry-eliding performance metric for NAC design. It decomposes any NAC into merely the mass of the neutron absorbing ^{10}B isotope per unit area. Geometry and other factors are removed and so disparate NACs can be readily compared using this metric. ^{10}BAD is given as:

$$^{10}\mathrm{BAD}\left[\mathrm{g\ cm^{-2}}\right] = \rho x w_p w_{\mathrm{B}} a_{^{10}\mathrm{B}} \tag{1}$$

where ρ is the composite mass density in g cm^{-2}, x is the composite's thickness in cm, w_p is the mass fraction of ^{10}B-containing particles, w_{B} is the mass fraction of B in those particles, and $a_{^{10}\mathrm{B}}$ is the isotopic abundance of ^{10}B in that B. Adjusting the estimated ^{10}BAD by altering composition and other factors like thickness can then design an effective NAC.[4]

Areal density including other constituents. Jiang et al. (2019) introduced the concept of equivalent boron areal density (EBAD) that includes absorption by additional particles or constituents. Thus, the complete

[2] Assumed to be the only absorbing nuclide in the standards.

[3] The flux depression resulting from this foil was neglected in calculations.

[4] Li et al. (2017) suggested at least 34 mg cm^{-2}.

absorptivity of a NAC – beyond its ^{10}B content alone – is accounted for. EBAD is given as:

$$\text{EBAD}\left[\text{g cm}^{-2}\right] = \rho x w_{\text{B}(eq.)} \tag{2a}$$

$$w_{\text{B}(eq.)} = w_{\text{B}} + \eta_{x,\text{B}} * w_x \tag{2b}$$

where $\eta_{x,\text{B}}$ is relative neutron absorptivity with respect to B and w_x is the mass fraction of the other absorbing constituent,[5] and $\eta_{x,\text{B}}$ is the relative absorption efficiency of the other absorbing constituent compared to B. The comparison is to natural B instead of ^{10}B, but ^{10}B or even another absorber could serve as the comparison. $\eta_{x,\text{B}}$ in Eq. (2b) is not merely the ratio of cross-sections. As atomic masses and densities differ between nuclides, a per-mass comparison is needed:

$$\eta_{x,\text{B}} = \frac{\sigma_x / M_x}{\sigma_{\text{B}} / w_{\text{B}}} \tag{3}$$

where σ is the microscopic cross-section and M is the molar mass of each constituent (Jiang et al., 2019).

Areal density including particle size effect. Neutron channeling reduces absorption efficiency, which can be accounted for by introducing an effect on absorber areal density based on particle size. This particle size effect is an effective macroscopic cross-section from the ratio of apparent macroscopic cross-section for a specific particle size to the bulk macroscopic cross-section for the homogeneous case. From previous work (O'Connor et al., 2020), the ^{10}BAD adjusted for the NAC particle size[6] is given as:

$$^{10}\text{BAD}_{\eta(d)}\left[\text{g cm}^{-2}\right] = \rho x w_{p,\eta} w_{\text{B}} a_{^{10}\text{B}} \tag{4a}$$

$$w_{p,\eta} = \sum_i w_i \cdot \eta_i(d) \tag{4b}$$

$$\eta(d) = \frac{\Sigma_t(d)}{\lim_{d\to 0} \Sigma_t} \tag{4c}$$

where w_i is the mass fraction of each particle i of a particular size, η_i is the relative efficacy of the size for particle i, and d is the average particle size. This exercise may be repeated for a range of particle sizes, particle compositions, and neutron energies.

Areal density including other constituents and particle size effect. Combining the particle size penalized-^{10}BAD and multi-component EBAD into one metric yields boron-10 equivalent areal density (^{10}BEAD). ^{10}BEAD may be computed as:

$$^{10}\text{BEAD}\left[\text{g cm}^{-2}\right] = \underbrace{\rho x w_{p,\eta} w_{p,^{10}\text{B}_{eq}}}_{\text{particle(s)}} + \underbrace{\rho x w_m w_{m,^{10}\text{B}(eq.)}}_{\text{matrix}} \tag{5}$$

where $w_{p,^{10}\text{B}_{eq}}$ and $w_{m,^{10}\text{B}_{eq}}$ are the ^{10}B-equivalent mass for the particle and matrix, respectively, and w_m is the mass fraction of the matrix. The particle size effect ($w_{p,\eta}$ from Eq. (4b)) is only applied to the particle component as the matrix is assumed homogeneous and not subject to any neutron channeling effects. Each component of ^{10}BEAD may be extended to include a number of additional neutron-absorbing constituents – like another particle or composition – or other even effects like a distribution of particle sizes or geometries.

A neutron-absorbing matrix reinforced with B_4C is notionally depicted in Fig. 4 to visualize the ^{10}BEAD metric. The final metric is then the sum of the contribution from particles – only their ^{10}B content, subject to a particle size effect represented by the missing portion of the pie chart – and from the matrix.

[5] Here, mass fractions are of the overall mass of the composite and not of their respective particles as in Eq. (1).

[6] Åkerhielm (1960) proposed a similar concept though this was apparently not adopted by subsequent literature.

3.2. Experimental measurements

The ASTM E2971-16 standard (E07 Committee, 2020) prescribes a number of corrections and considerations for measuring the areal density of a neutron absorber. The measured count rate must be adjusted for changes in the power of the incident neutron beam[7] and background & non-thermal neutron counts.[8] To account for effects such as spectral hardening, measured counts are compared to those from calibration standards in order to compute the measured areal density. Instead of reporting a reduction in counts that can be affected by factors unique to a particular experimental setup or even individual exposure, this standard instead reports a specimen's ability to absorb thermal neutrons as a ^{10}BAD measurement.[9]

The existing In foil activation setup at NASA Langley Research Center (LaRC) (Kang et al., 2015; Bacca et al., 2022) used a single foil to measure the neutrons transmitted through an irradiated specimen was modified by the addition of a second In foil just before the irradiated specimen that enabled correction for changing incident neutron flux. This correction allowed for comparisons between different exposures while obviating the effects of typical alignment and distance errors. A strong neutron absorber was used to determine the counts arising from background radiation and non-thermal neutrons. If these counts were attributed to thermal neutron absorption, then specimens could falsely appear to be more effective in the thermal range. The directing counting setup was more similar to that detailed in the ASTM standard, requiring minimal modification.

4. Results

Over the first centimeter through a prototypical NAC, the simulated neutron transmission ratio shown in Fig. 5 for particles in the tens of microns, micron, and sub-micron ranges rapidly diverges. Particles larger than tens of microns show a rapid increase in transmission relative to the 60 nm case, indicating reduced absorption efficiency. Conversely, the trend for sub-micron particles is indistinguishable, showing no neutron channeling. For the micron range, particles are initially nearly as efficient as sub-micron ones. The 10 μm particles remain less than 25% divergent until about 0.5 cm. By 1 cm, however, only 1 μm and below are less than 20% divergent.

Fig. 6 compares the relative absorbing efficacy by particle size for multiple analytical models compared to the present work's simulations. The analytical and simulation results give substantially equivalent results. Based on the line of best fit to simulation results, it appears that 10 μm particles are at least 95% as efficient as the homogeneous case. 100 μm particles are still over 80% efficient. By 1000 μm, the efficiency drops precipitously.

The relative efficiency by particle size depicted in Fig. 7 appears constant at a range of typical reinforcement volume fractions. However, the particle sizes penalty increases in absolute terms with increasing volume fraction.

Fig. 8 shows that matrices that inherently absorb neutrons (*e.g.* Mg–14*wt*%Li, LA141) demonstrated a somewhat lessened penalty but the difference was small in absolute terms.

[7] For instance, from a slight, unintentional change in positioning of the source or specimen holder or even a substantial decay in the neutron source activity between exposures.

[8] For instance, background from immutable external or cosmic sources. And for non-thermal counts, from polyenergetic neutron sources and/or a detector sensitive to higher energy neutrons.

[9] One could say "This specimen absorbs thermal neutrons as if it had x mg cm^{-2} of ^{10}B".

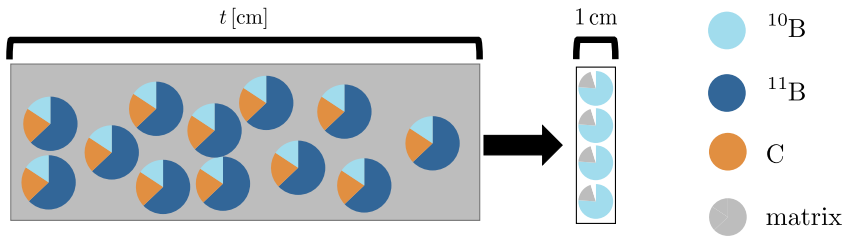

Fig. 4. Diagram showing decomposition of a NAC into its components that contribute to ^{10}BEAD.

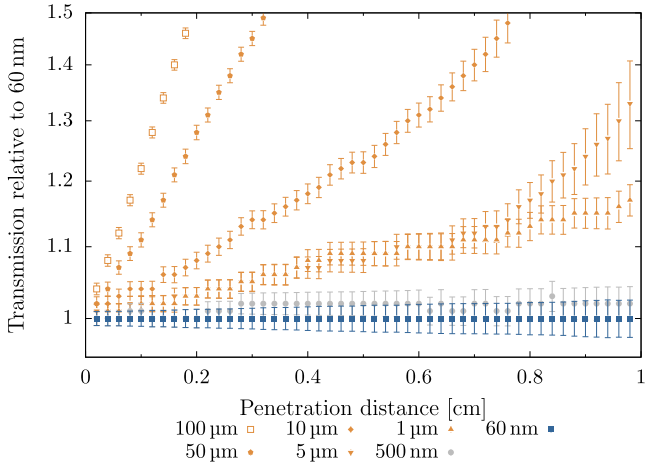

Fig. 5. Relative neutron transmission for various particles sizes compared to 60 nm, indicating that particles larger than a few microns rapidly diverge.

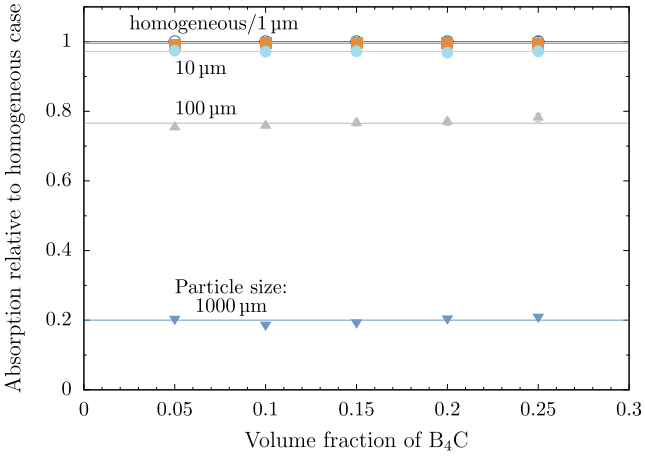

Fig. 7. Relative macroscopic cross-section for several particle sizes, indicating that the neutron channeling penalty is fairly invariant with respect to volume fraction for the dilute case.

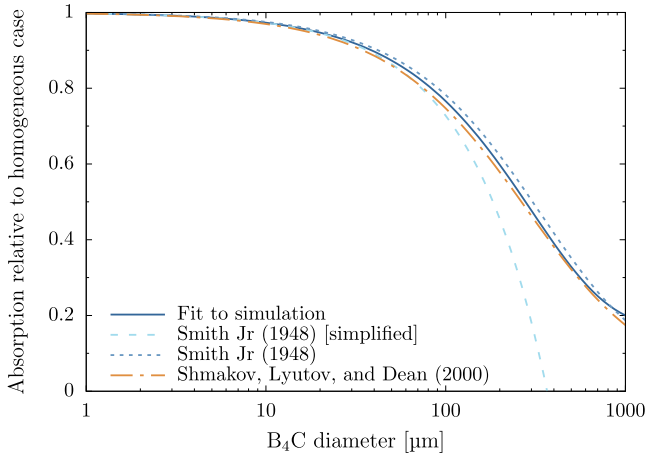

Fig. 6. Macroscopic cross-section by particle size from analytical models compares favorably to this study's simulations.

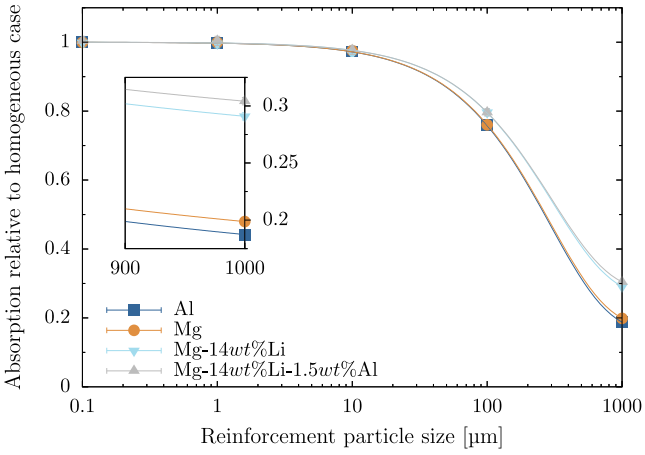

Fig. 8. Relative macroscopic cross-section by particle size for several matrices, showing a reduction in channeling at large particle sizes for absorbing matrices.

4.1. Areal density performance metrics

Li et al. (2017) claimed that a composite with 34 mg cm^{-2} ^{10}BAD would block 99% of thermal neutrons. Using this recommendation for ^{10}BEAD, the mass reduction of matrix substitution for a B_4C NAC can be estimated as demonstrated in Fig. 9. Substituting less dense Mg for Al, the predicted mass reductions are close to that from mass density reduction alone. With increasing reinforcement volume fraction, the predicted mass reduction somewhat decreases although 80% of the maximum savings are retained at 25% B_4C by volume. The mass reduction for Mg substitution ranges from 25% to 35% over Al. Substituting an absorbing Mg–14*wt*%Li matrix,[10] the predicted mass reductions at low volume fractions are even greater than that from mass density reduction alone. The decrease in mass reduction with increasing volume fraction is, however, more rapid than seen for the Mg substitution. The mass reduction for Mg–14*wt*%Li substitution ranges from 20% to 40% over Mg and from 40% to 60% over Al.

[10] Assuming a ^{6}Li abundance of 7.59%.

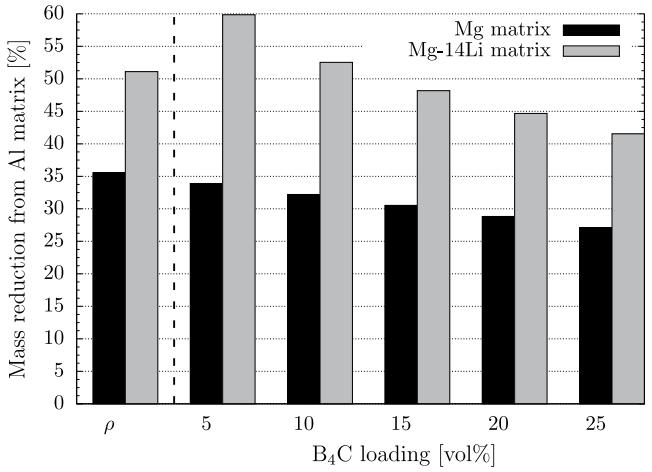

Fig. 9. Relative mass reduction from substituting Mg/Mg–14*wt*%Li for Al in B_4C-reinforced composites by reinforcement volume fraction with respect to neutron absorptivity.

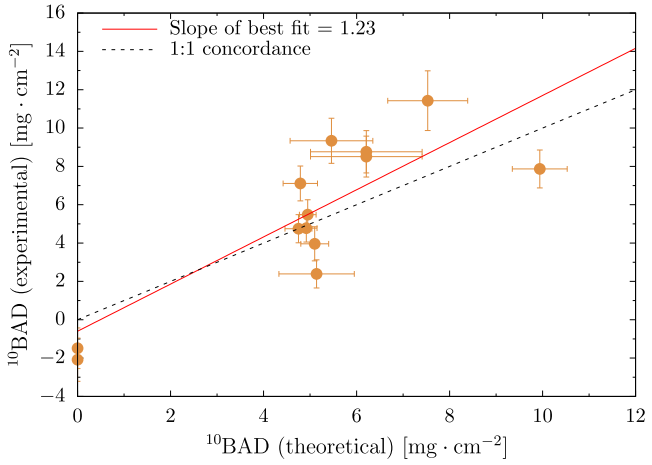

Fig. 10. Only considering the particle contribution to the areal density underpredicts the measured areal density.

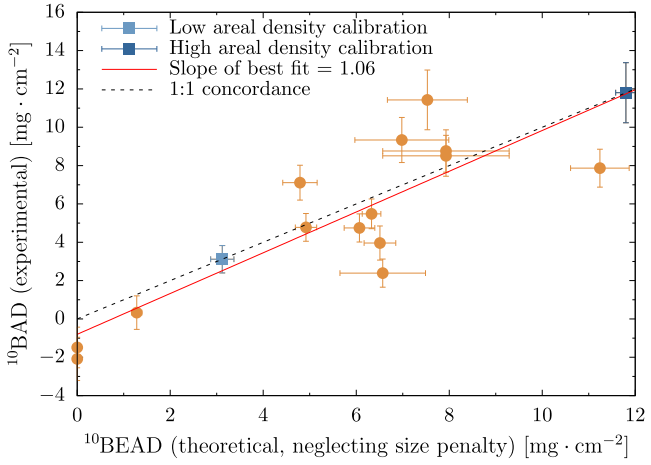

Fig. 11. Considering both the matrix and particle contributions to areal density improves predictions.

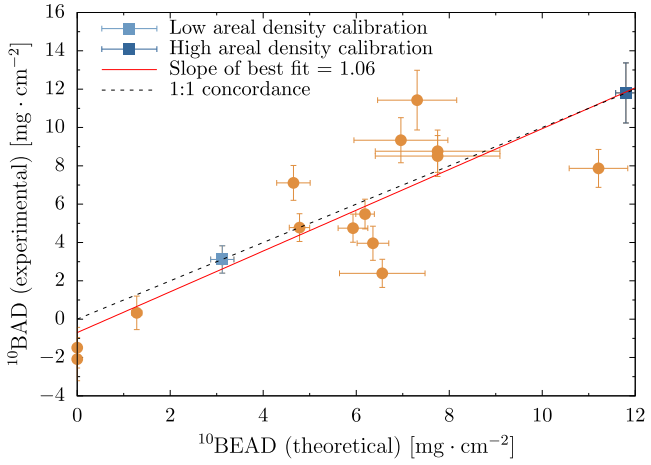

Fig. 12. Areal density estimated using matrix and particle contributions, including the particle size effect, reasonably predicts areal density measured by the foil activation setup.

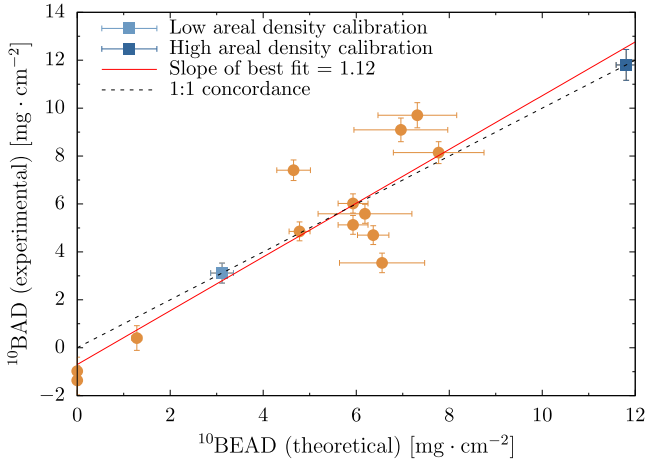

Fig. 13. Areal density predictions are also reasonable for the direct counting setup.

4.2. Experimental

For the foil activation method, only considering the particle's contribution to areal density underpredicted ^{10}BAD as shown in Fig. 10. Including the matrix contribution to areal density better predicted the measured areal density as indicated by Fig. 11. Including the particle size effect did not substantially alter the predictions as shown in Fig. 12. For the direct counting method, considering the particle contribution alone again underpredicted measured areal density ^{10}BAD as shown by the 1:1 concordance line being substantially under the experimental trendline. Fig. 13 shows that considering both the matrix contribution and the particle size effect in ^{10}BEAD improved the concordance between estimated and measured areal densities.

5. Discussion

5.1. Analytical models and simulations

Previous computational models of NACs were periodic arrangements of absorbing particles (Kim et al., 2014; Soltani et al., 2016) or did not closely investigate particle sizes smaller than a micron (Sun et al., 2020). This study instead used a physically realistic pseudo-random distribution of particles within the modeled NAC while sampling down to nanoscale particle sizes. Pseudo-random sublattices with

100 cells in each dimension were found to be reasonably accurate and without excessive computational burden. Neutron channeling is evident when tracking neutrons transmitted through the first centimeter of a pseudo-random NAC model. However, a reasonably effective NAC will absorb most incident neutrons within the first few millimeters. Provided that incident fluence is not excessive, then – for sufficiently small particles like 10 μm or less – neutron channeling will only be a concern for the first few millimeters into a NAC. After this distance, there still will be some reduction in shielding efficiency due to channeling. However, the absolute neutron fluence may be so low (due to previous absorption) that any reduction in shielding efficiency is insubstantial.

The studied analytical models do not consider scattering in their calculations. It was initially supposed that scattering in the matrix or reinforcement would increase the distance any one neutron would expect to traverse within the NAC and that this increase would result in additional absorption, reducing the effect of neutron channeling. As PHITS does compute scattering, it was thought that simulations might show a lessened particle size effect or, rather, the penalty being relegated to even larger particle sizes. As shown by the excellent agreement between analytical models and this work's simulation results, the influence of scattering is apparently negligible under the studied conditions. However, a more strongly scattering matrix – *e.g.* hydrogenous polymers – may exhibit such a reduction in neutron channeling.

5.1.1. Particle size effect

The studied analytical models, some previous literature reports, and this work's simulations found a consistent trend of the particle size effect beginning to be noticeable around 10 μm and especially substantial after 100 μm for B_4C particles, without much regard to volume fraction. Schrempp-Koops (2013) used a different analytical model to find that shielding efficiency was preserved well through 1 μm and fell off rapidly as particle size exceeded 10 μm, agreeing fairly well with this study. DiJulio et al. (2018) experimentally found a rather small effect of B_4C particle size on reinforced concrete when the particles were smaller than 63 μm, which comports with the present study. Wells et al. (1987) found that Boral was 82.5% as effective as the homogeneous case when B_4C particles were 130 μm, again similar to this study. Turner (2005) found that 10 μm B_4C exhibited a particle size effect of less than 5% and only past 100 μm was the penalty more than 25%. However, that study found a linear trend with increasing particle size whereas most other studies, including this one, found an exponential trend. Conversely, Wells and Hobbes (2005) found the particle size effect was effectively zero up to 150 μm. Their lack of penalty is inconsistent with this study but the critical size for the penalty is consistent. Recently, some literature reports suggested that nano- or sub-micron-size particles were necessary to avoid the channeling effect in NACs (Kim et al., 2014; Sun et al., 2020; El-Khatib et al., 2021; Soltani et al., 2016). However, these reports did not closely study the sub-micron or micron particle size regimes, compared based on other measures than neutron absorptivity, or used polymeric matrices that could enhance moderation and scattering. Indeed, El-Khatib et al. (2021) found an inverse neutron channeling effect with respect to particle size[11] – where nano-sized particles performed worse. Overall, there is agreement between analytical models, this study's simulations, and experimental results on the critical particle size – at which channeling has a substantial effect – lying between 10 μm to 100 μm for B_4C NACs where the matrix is not highly scattering. This size is near the mean free path of about 120 μm for thermal neutrons in B_4C.

[11] This may instead be due to micron-size particles leading to more channeling through a highly moderating and scattering polymeric matrix. Therefore, an apparent increase in thermal neutron fluence for the nano-sized case is not from less absorption but rather from increased moderation and scattering.

5.2. Using boron-10 equivalent areal density as a performance metric

The mass reduction for a NAC from substituting one non-absorbing matrix with another appears limited to the difference in mass density and inversely proportional to the matrix volume fraction. For instance, Mg provides lightweighting by reduction in mass density alone — accordingly, this substitution is less effective at high reinforcement volume fractions as there is less matrix mass to be reduced. The absorbing particles are not affected and do not participate in the lightweighting. Therefore, there is an inherent limit to lightweighting determined by the mass density difference.

When lightweighting NACs by substituting a neutron absorbing matrix such as Mg–Li, both the substituted matrix's neutron absorptivity and mass density difference influence the mass reduction. For dilute reinforcement, the mass reduction from absorbing matrix substitution exceeds that expected from mass density alone. It is not limited by mass density differences as for non-absorbing matrices. The inherently absorbing matrix displaces a portion of the absorptivity needed from the denser reinforcement, ultimately reducing overall mass density.

5.3. Experimental

There is substantial uncertainty in the measured ^{10}BAD from foil activation, which arises from Poisson statistics of the number of counts of the foils. The relative uncertainty per 100 s count immediately after the foils were removed from the exposure was about 2%. However, the exponential decay in counts resulted in a relative uncertainty nearer 5% towards the end of the counting period. Additional uncertainty was introduced from the fairly high background count rate – only 1% of the foil's count at the beginning of the counting period but rising to 6% by the end – and removal of non-thermal neutrons. Only about half of the counts were attributable to thermal neutrons, which introduced substantial uncertainty into eventual measured ^{10}BAD, especially for specimens like the high areal density calibration standard where counts were inherently lower due to its substantial absorption. As such, there is substantial uncertainty in the comparison of measured to estimated areal density. However, the linear trendline shows a correlation once all predictive terms are used to calculate ^{10}BEAD, indicating this technique's validity. The introduction of corrections for incident neutron flux, background radiation, and non-thermal neutron counts improved the accuracy of this setup.

For the direct counting setup, about 80% of counts were apparently from background and non-thermal neutrons. The exposure room had a low background when the source was not present, so this intense population of background and non-thermal neutrons probably occurred due to the neutron emitted isotropically from the barrel being scattered by the surroundings into the detector. Ostensibly, the Cd wrapping around the detector was insufficient to prevent this. Yet this technique had lower uncertainty in measured ^{10}BAD than the foil activation one. The longer time for counting made the total number of counts much greater, reducing counting uncertainty by Poisson statistics. This technique may slightly underpredict measured areal density but demonstrates the utility of this technique combined with ^{10}BEAD.

6. Conclusions

Overall, this study found good agreement between analytical models and a physically representative simulations of neutron channeling in NACs, supporting the use of micron-sized absorbing particles. It also introduced a more comprehensive NAC design metric: ^{10}BEAD. And it provided experimental validation for ^{10}BEAD using two different measurement techniques. Analytical models from literature and a physically representative simulation found that for a B_4C-reinforced NAC, particles less than 100 μm and especially those less than 10 μm do not lead to excessive neutron channeling. The boron-10 equivalent areal density (^{10}BEAD) metric was developed to more comprehensively

estimate NACs performance by considering both matrix contribution and the particle size effect. Lightweighting calculations using ^{10}BEAD showed that overall mass reduction is limited to the mass density difference for a non-absorbing matrix such as Mg but it is greater than that from mass density differences alone for an absorbing matrix such as Mg–Li. The utility of ^{10}BEAD was validated by comparing measured ^{10}BAD versus expected ^{10}BEAD. An In foil activation setup for neutron absorption testing was modified to account for changes in incident neutron flux, background radiation, and non-thermal neutron counts. Using this setup, measured ^{10}BAD correlated with expected ^{10}BEAD, considering both the contribution from an absorbing matrix and the penalty from particle size. A separate direct counting setup supported these findings.

6.1. Limitations and future work

The influence of moderation and scattering by matrix and by reinforcement,[12] should be investigated with respect to neutron channeling. Previously proposed NACs effective at higher energies used both moderating hydrides and absorbing borides (Poindexter et al., 1966; Poindexter, 1967), necessitating understanding of such effects if such technology is to be recaptured.

^{10}BEAD could be extended to different matrix compositions and even multiple particle compositions, geometries, or sizes. These lightweighting calculations only considered Al, Mg, and Mg–14wt%Li matrices homogeneously reinforced by B_4C. Other reinforcements that are less mass dense than even the matrix like LiH should be considered.

Potential changes to the neutron absorption testing setups include reducing uncertainties and extending their capabilities. For both setups, reducing the background component through means such as additional shielding or longer counting periods would improve statistics. By adjusting the moderating power of each setup and employing a fast neutron detector or Bonner spheres, the absorptivity of NACs at higher neutron energies could additionally be investigated.

There are a number of reasons for the underprediction of neutron absorber areal density in these specimens. The isotopic abundance of ^{6}Li in the fabricated specimen was assumed, and is liable to change depending on the source of the Li. The amount of absorbing particles in the composites could be inhomogeneous (Park et al., 2020). Additionally, the particles may be agglomerated or clustered, reducing apparent neutron absorption (Zhai et al., 2021).

CRediT authorship contribution statement

Andrew O'Connor: Writing – original draft, Visualization, Software, Methodology, Investigation, Funding acquisition, Conceptualization. **Cheol Park:** Writing – review & editing, Supervision, Resources, Methodology. **Wesley E. Bolch:** Writing – review & editing, Conceptualization. **Andreas Enqvist:** Writing – review & editing, Resources, Methodology. **Michele V. Manuel:** Writing – review & editing, Supervision, Resources, Project administration, Funding acquisition.

Declaration of competing interest

The authors declare the following financial interests/personal relationships which may be considered as potential competing interests: This work was supported by a NASA Space Technology Research Fellowship (award 80NSSC19K1163).

Data availability

Data will be made available on request.

[12] LiH for example, readily moderates and absorbs neutrons.

Acknowledgments

This work was supported by a NASA, United States Space Technology Research Fellowship (award 80NSSC19K1163). Any opinions, findings, and conclusions or recommendations expressed in this material are those of the author(s) and do not necessarily reflect the views of the National Aeronautics and Space Administration. Thanks to Dr Sang-Hyon Chu and to Ms Calista Lum for their assistance in setting up the foil activation experiments at NASA LaRC. Thanks to Mr Caleb Schenck for collecting some of the neutron absorption data at UF.

References

Afkham, Y., Mesbahi, A., Alemi, A., Zolfagharpour, F., Jabbari, N., 2020. Design and fabrication of a Nano-based neutron shield for fast neutrons from medical linear accelerators in radiation therapy. Radiat. Oncol. 15, http://dx.doi.org/10.1186/s13014-020-01551-1.

Åkerhielm, F., 1960. Transmission of Thermal Neutrons through Boral. Technical Report AE-24, Aktiebloaget Atomenergi, Stockhol, Sweden.

Athanasakis, M., Ivanov, E., del Rio, E., Humphry-Baker, S.A., 2020. A high temperature W2B–W composite for fusion reactor shielding. J. Nucl. Mater. 532, 152062. http://dx.doi.org/10.1016/j.jnucmat.2020.152062.

Bacca, N., Zhang, C., Paul, T., Sukumaran, A.K., John, D., Rengifo, S., Park, C., Chu, S.-H., Mazurkivich, M., Scott, W., Agarwal, A., 2022. Tribological and neutron radiation properties of boron nitride nanotubes reinforced titanium composites under lunar environment. J. Mater. Res. 37, 4582–4593. http://dx.doi.org/10.1557/s43578-022-00708-w.

Basturk, M., Kardjilov, N., Lehmann, E., Zawisky, M., 2005. Monte Carlo simulation of neutron transmission of boron-alloyed steel. IEEE Trans. Nucl. Sci. 52, 394–399. http://dx.doi.org/10.1109/TNS.2005.843638.

Belvin, W.K., Watson, J.J., Singhal, S.N., 2006. Structural concepts and materials for lunar exploration habitats. In: Collection of Technical Papers - Space 2006 Conference. Vol. 3, American Institute of Aeronautics and Astronautics, San Jose, CA, pp. 1666–1680. http://dx.doi.org/10.2514/6.2006-7338.

Burrus, W.R., 1958. How channeling between chunks raises neutron transmission through boral. Nucleonics 16, 91–94.

Burrus, W.R., 1960. Radiation Transmission through Boral and Similar Heterogeneous Materials Consisting of Randomly Distributed Absorbing Chunks. Technical Report ORNL-2528, Oak Ridge National Laboratory, Oak Ridge, TN, http://dx.doi.org/10.2172/4196641.

Caffrey, J.A., Gomez, C.F., Scharber, L.L., 2015. Shielding development for nuclear thermal propulsion. In: Nuclear and Emerging Technologies for Space. NETS, American Nuclear Society, Albuquerque, NM, p. 12, URL: https://ntrs.nasa.gov/citations/20150006884.

Cecchetto, M., Garcia Alia, R., Wrobel, F., Tali, M., Stein, O., Lerner, G., Bilko, K., Esposito, L., Bahamonde Castro, C., Kadi, Y., Danzeca, S., Brucoli, M., Cazzaniga, C., Bagatin, M., Gerardin, S., Paccagnella, A., 2020. Thermal neutron-induced SEUs in the LHC accelerator environment. IEEE Trans. Nucl. Sci. 67, 1412–1420. http://dx.doi.org/10.1109/TNS.2020.2997992.

Chen, H.-S., Wang, W.-X., Li, Y.L., Zhang, P., Nie, H.H., Wu, Q.C., 2015. The design, microstructure and tensile properties of B4C particulate reinforced 6061Al neutron absorber composites. J. Alloys Compd. 632, 23–29. http://dx.doi.org/10.1016/J.JALLCOM.2015.01.048.

Chen, H.S., Wang, W.X., Li, Y.L., Zhou, J., Nie, H.H., Wu, Q.C., 2016. The design, microstructure and mechanical properties of B4C/6061Al neutron absorber composites fabricated by SPS. Mater. Des. 94, 360–367. http://dx.doi.org/10.1016/J.MATDES.2016.01.030.

DiJulio, D.D., Cooper-Jensen, C.P., Llamas-Jansa, I., Kazi, S., Bentley, P.M., 2018. Measurements and Monte-Carlo simulations of the particle self-shielding effect of B4C grains in neutron shielding concrete. Radiat. Phys. Chem. 147, 40–44. http://dx.doi.org/10.1016/j.radphyschem.2018.01.023.

Dyrnjaja, E., Zawisky, M., 2015. The influence of boron micro-inhomogeneities on neutron transmission. Nucl. Instrum. Methods Phys. Res. B 347, 47–51. http://dx.doi.org/10.1016/J.NIMB.2015.01.052.

E07 Committee, 2020. Test Method for Determination of Effective Boron-10 Areal Density in Aluminum Neutron Absorbers using Neutron Attenuation Measurements. Technical Report E2971-16, ASTM International, West Conshohocken, PA, http://dx.doi.org/10.1520/E2971-16R20.

El-Khatib, A.M., Hamada, M.S., Alabsy, M.T., Youssef, Y.M., Elzaher, M.A., Badawi, M.S., Fayez-Hassan, M., Kopatch, Y.N., Ruskov, I.N., Abbas, M.I., 2021. Fast and thermal neutrons attenuation through micro-sized and nano-sized CdO reinforced HDPE composites. Radiat. Phys. Chem. 180, 109245. http://dx.doi.org/10.1016/j.radphyschem.2020.109245.

Fu, X., Ji, Z., Lin, W., Yu, Y., Wu, T., 2021. The advancement of neutron shielding materials for the storage of spent nuclear fuel. Sci. Technol. Nucl. Install. 2021, e5541047. http://dx.doi.org/10.1155/2021/5541047.

ICRP, 2013. ICRP publication 123: Assessment of radiation exposure of astronauts in space. Ann. ICRP 42, http://dx.doi.org/10.1016/j.icrp.2013.05.004.

ICRP, 2016. ICRP publication 132: Radiological protection from cosmic radiation in aviation. Ann. ICRP 45, http://dx.doi.org/10.1177/ANIB_45_1.

Jiang, L.T., Xu, Z.G., Fei, Y.K., Zhang, Q., Qiao, J., Wu, G.H., 2019. The design of novel neutron shielding (Gd+B4C)/6061Al composites and its properties after hot rolling. Composites B 168, 183–194. http://dx.doi.org/10.1016/J.COMPOSITESB.2018.12.087.

Kang, J.H., Sauti, G., Park, C., Yamakov, V.I., Wise, K.E., Lowther, S.E., Fay, C.C., Thibeault, S.A., Bryant, R.G., 2015. Multifunctional electroactive nanocomposites based on piezoelectric boron nitride nanotubes. ACS Nano 9, 11942–11950. http://dx.doi.org/10.1021/acsnano.5b04526.

Kim, J., Lee, B.-C., Uhm, Y.R., Miller, W.H., 2014. Enhancement of thermal neutron attenuation of nano-B4C, -BN dispersed neutron shielding polymer nanocomposites. J. Nucl. Mater. 453, 48–53. http://dx.doi.org/10.1016/J.JNUCMAT.2014.06.026.

Lee, D., Kim, J., Park, B., Jo, I., Lee, S.-K., Kim, Y., Lee, S.-B., Cho, S., 2021. Mechanical and thermal neutron absorbing properties of B4C/Aluminum Alloy Composites Fabricated by stir casting and hot rolling process. Metals 11, 413. http://dx.doi.org/10.3390/met11030413.

Li, Y., Wang, W.-X., Zhou, J., Chen, H.-S., Zhang, P., 2017. 10B areal density: A novel approach for design and fabrication of B4C/6061Al neutron absorbing materials. J. Nucl. Mater. 487, 238–246. http://dx.doi.org/10.1016/J.JNUCMAT.2017.02.020.

Machiels, A., Lambert, R., 2009. Handbook of Neutron Absorber Materials for Spent Nuclear Fuel Transportation and Storage Applications: 2009 Edition. Technical Report Final report, Electric Power Research Institute, Palo Alto, CA.

Malaki, M., Xu, W., Kasar, A., Menezes, P., Dieringa, H., Varma, R., Gupta, M., 2019. Advanced metal matrix nanocomposites. Metals 9, 330. http://dx.doi.org/10.3390/met9030330.

Naito, M., Kitamura, H., Koike, M., Kusano, H., Kusumoto, T., Uchihori, Y., Endo, T., Hagiwara, Y., Kiyono, N., Kodama, H., Matsuo, S., Mikoshiba, R., Takami, Y., Yamanaka, M., Akiyama, H., Nishimura, W., Kodaira, S., 2021. Applicability of composite materials for space radiation shielding of spacecraft. Life Sci. Space Res. 31, 71–79. http://dx.doi.org/10.1016/j.lssr.2021.08.004.

O'Connor, A., Bolch, W.E., Manuel, M.V., 2020. Lightweight radiation shielding using metal matrix composite. In: TMS 2020: Metal-Matrix Composites: Analysis, Modeling, Observations and Interpretations. TMS, San Diego, CA.

O'Connor, A., Park, C., Baciak, J.E., Manuel, M.V., 2024. Mitigating space radiation using magnesium(-lithium) and boron carbide composites. Acta Astronaut. 216, 37–43. http://dx.doi.org/10.1016/j.actaastro.2023.12.013.

Park, J.-J., Hong, S.-M., Lee, M.-K., Rhee, C.-K., Rhee, W.-H., 2015. Enhancement in the microstructure and neutron shielding efficiency of sandwich type of 6061Al–B4C composite material via hot isostatic pressing. Nucl. Eng. Des. 282, 1–7. http://dx.doi.org/10.1016/J.NUCENGDES.2014.10.020.

Park, B., Lee, D., Jo, I., Lee, S.B., Lee, S.K., Cho, S., 2020. Automated quantification of reinforcement dispersion in B4C/Al metal matrix composites. Composites B 181, 107584. http://dx.doi.org/10.1016/j.compositesb.2019.107584.

Poindexter, A.M., 1967. Aluminum—Titanium Hydride—Boron Carbide Composite Provides Lightweight Neutron Shield Material. Tech Brief 67-10265, Westinghouse Astronuclear Laboratory, Large, PA, URL: https://ntrs.nasa.gov/search.jsp?R=19670000265.

Poindexter, A.M., Ricks, L., Disney, R., 1966. A Survey of Potential Shield Materials. Technical Report WANL-TME-1345, Westinghouse Astronuclear Laboratory.

Sato, T., Iwamoto, Y., Hashimoto, S., Ogawa, T., Furuta, T., Abe, S.-i., Kai, T., Tsai, P.-E., Matsuda, N., Iwase, H., Shigyo, N., Sihver, L., Niita, K., 2018. Features of particle and heavy ion transport code system (PHITS) version 3.02. J. Nucl. Sci. Technol. 55, 684–690. http://dx.doi.org/10.1080/00223131.2017.1419890.

Schrempp-Koops, L., 2013. Size effects on the efficiency of neutron shielding in nanocomposites-A full-range analysis. Int. J. Nanosci. 12, http://dx.doi.org/10.1142/S0219581X13500154.

Shmakov, V.M., Lyutov, V.D., Dean, V.F., 2000. Effective cross sections for calculations of criticality of dispersed media. In: PHYSOR 2000. Pittsburgh, PA, p. 26.

Singleterry, R.C., Thibeault, S.A., 2000. Materials for Low-Energy Neutron Radiation Shielding. Technical Report NASA/TP-2000-210281, NASA/LaRC, Hampton, VA, URL: https://ntrs.nasa.gov/citations/20000057013.

Smith, Jr., N.M., 1948. The Absorption and Scattering of Radiation in Random Aggregates of Pebbles. Final CNL-21(rev), Oak Ridge National Laboratory, Oak Ridge, TN.

Soltani, Z., Beigzadeh, A., Ziaie, F., Asadi, E., 2016. Effect of particle size and percentages of Boron carbide on the thermal neutron radiation shielding properties of HDPE/B4C composite: Experimental and simulation studies. Radiat. Phys. Chem. 127, 182–187. http://dx.doi.org/10.1016/J.RADPHYSCHEM.2016.06.027.

Sun, W., Hu, H., Yu, B., Sheng, L., Hu, G., Cai, Y., Yang, Q., Zhang, M., Yan, Y., 2020. Random model for radiation shielding calculation of particle reinforced metal matrix composites and its application. Appl. Radiat. Isot. 166, http://dx.doi.org/10.1016/j.apradiso.2020.109299.

Tamayo, P., Thomas, C., Rico, J., Cimentada, A., Setién, J., Polanco, J., 2020. Review on neutron-absorbing fillers. In: Micro and Nanostructured Composite Materials for Neutron Shielding Applications. Elsevier, pp. 25–52. http://dx.doi.org/10.1016/B978-0-12-819459-1.00002-7.

Thibeault, S.A., Kang, J.H., Sauti, G., Park, C., Fay, C.C., King, G.C., 2015. Nanomaterials for radiation shielding. MRS Bull. 40, 836–841. http://dx.doi.org/10.1557/mrs.2015.225.

Turner, S.E., 2005. Reactivity effects of streaming between discrete boron carbide particles in neutron absorber panels for storage or transport of spent nuclear fuel. Nucl. Sci. Eng. 151, 344–347. http://dx.doi.org/10.13182/NSE05-A2553.

Wells, A.H., Hobbes, J.S., 2005. Neutron Transmission through Boral: Impact of Channeling on Criticality. Technical Report Final report, Electric Power Research Institute, Palo Alto, CA.

Wells, A., Marnon, D., Karam, R., 1987. Criticality effect of neutron channeling between boron carbide granules in boral for a spent-fuel shipping cask. In: Transactions of the American Nuclear Society. American Nuclear Society, Dallas, TX, pp. 205–206.

Yamamoto, T., 2006. Extension of cross section homogenization method for particle-dispersed media to layered particles. Ann. Nucl. Energy 33, 804–812. http://dx.doi.org/10.1016/j.anucene.2006.04.004.

Yamamoto, T., 2010. Study on double heterogeneity effect of Pu-rich agglomerates in mixed oxide fuel using cross section homogenization method for particle-dispersed media. Ann. Nucl. Energy 37, 398–405. http://dx.doi.org/10.1016/j.anucene.2009.11.016.

Yamamoto, T., Miyoshi, Y., Takeda, T., 2006. Extension of effective cross section calculation method for neutron transport calculations in particle-dispersed media. J. Nucl. Sci. Technol. 43, 77–87. http://dx.doi.org/10.1080/18811248.2006.9711069.

Zhai, H., Zhong, S., Li, J., Chen, Y., Cui, Y., Chen, Z., Sun, G., Wang, H., 2021. The neutron shielding modeling and experimental characteristic in TiB2/Al composites. Mater. Today Commun. 27, 102194. http://dx.doi.org/10.1016/j.mtcomm.2021.102194.

Zhang, P., Li, Y.-L., Wang, W.-X., Gao, Z., Wang, B., 2013. The design, fabrication and properties of B4C/Al neutron absorbers. J. Nucl. Mater. 437, 350–358. http://dx.doi.org/10.1016/J.JNUCMAT.2013.02.050.

Zhang, P., Li, J., Wang, W.-x., Tan, X.-y., Xie, L., Guo, F.-y., 2019. The design, microstructure and mechanical properties of a novel Gd2O3/6061Al neutron shielding composite. Vacuum 162, 92–100. http://dx.doi.org/10.1016/J.VACUUM.2019.01.004.